ELSEVIER

International Journal of Mass Spectrometry 217 (2002) 23–44

International Journal of Mass Spectrometry

www.elsevier.com/locate/ijms

Why are smaller fragments preferentially lost from radical cations at low energies and larger ones at high energies? An experimental and theoretical study

Lawrence L. Griffin[a], John C. Traeger[b], Charles E. Hudson[c], David J. McAdoo[c,*]

[a] *Department of Marine Sciences, Texas A&M University at Galveston, Galveston, TX 77553, USA*
[b] *Department of Chemistry, La Trobe University, Bundoora 3083, Vic., Australia*
[c] *Department of Human Biochemistry & Genetics, Marine Biomedical Institute, University of Texas Medical Branch, 301 University Boulevard, Galveston, TX 77555-1043, USA*

Received 22 June 2001; accepted 1 October 2001

Abstract

A long-standing mystery in gas phase ion chemistry is: why are smaller fragments preferentially lost at low energies and larger fragments at higher energies in competing α-cleavages? This is addressed here by studies of dissociations of ethanol, 2-propanol, 2-butanol, 2-methylpropane and 2-butanone radical cations. The onsets and energy dependencies of the reactions were obtained by photoionization mass spectrometry. Stationary point geometries, critical energies and vibrational frequencies were generated by B3LYP/6-31G(d) and B3LYP/6-311G(d,p) theory (DFT). Dependencies of reaction rates on internal energy were calculated by Rice–Ramsperger–Kassel–Marcus (RRKM) theory. Results obtained establish the generality of a previous finding that loss of $H^{\bullet}$ is slower than competing losses of polyatomic fragments. This is attributable to substantial lowering of the frequencies of the vibrations that are converted to rotations and translations in the transition states for the latter reactions, but not in transition states for $H^{\bullet}$ losses. It is concluded that lower dissociation thresholds produce preferred losses of smaller alkyl fragments at low energies and that looser transition states favor losses of larger fragments at higher energies. DFT results and abundances of parallel alkane eliminations (two step processes also initiated by simple CC bond cleavage) indicate that cleavage of the CC bond to the larger alkyl fragment is most frequent even below the threshold for complete dissociation (energies at which ion-induced dipole alkyl complexes are formed), i.e., at all energies of bond cleavage, even if not reflected in simple cleavage abundances near threshold. Obtaining realistic rates by RRKM theory required increasing the lowest transition state vibrational frequencies (for modes that become rotations and translations) to well above those obtained by DFT for alkyl losses, further evidence that the rates of those reactions are controlled by minimum entropy transition states occurring earlier than the single imaginary frequency transition states found by DFT. In addition, comparison of DFT critical energies, photoionization critical energies and critical energies that give the best RRKM rates support relaxation of the ground states to lower energy species with long CC bonds following ionization. Preferred losses of larger alkanes at low energies, dominant losses of larger alkyl groups at high energies and formation of long CC bonds to the larger alkyl in the ground state ion all appear to have a common origin. (Int J Mass Spectrom 217 (2002) 23–44) © 2002 Elsevier Science B.V. All rights reserved.

Keywords: Density functional theory; Photoionization mass spectrometry; RRKM theory; Size effects; Transition states

* Corresponding author. E-mail: djmcadoo@utmb.edu

PII S1387-3806(02)00529-8

1. Introduction

This work is dedicated to the memory of Pierre Longevialle and his many fine contributions to our understanding of gas phase ion chemistry. Of particular note is his discovery that fragments from one end of an ionized steroid can move many angstroms to the other end and react there [1,2] and his later extensions of those results to other systems [3,4]. Following up on Pierre's seminal contributions, much work over the past two decades has shown that CC bonds in ions in the gas phase can break to form electrostatically bound ion–neutral complexes below the threshold for complete dissociation [5–9]. We will miss him in gas phase ion chemistry. Present work reveals that the preference for loss of larger alkyl groups from a given radical cation at high energies is related to effects of fragment size investigated by Longevialle [4].

Early work demonstrated that in the α-cleavages of radical cations in the gas phase, larger alkyl groups are lost more abundantly than are hydrogen atoms and smaller alkyls [10]. However, closer scrutiny revealed that, while larger fragments are preferentially lost at high energies, smaller ones are preferentially lost from the same molecular ion at low energies [11,12]. This pattern holds in the dissociations of ionized straight chain aliphatic ketones, Schiff bases, aliphatic ethers (excluding losses of $CH_3^{\bullet}$ from the latter ions) [11], ketals [12], γ,γ-dialkylallyl methyl ethers [13] and secondary amines [4].

Maccoll demonstrated that losses of smaller alkyl fragments are favored near threshold because those processes have lower critical energies [14]. He further noted that, starting from a value of about 1.0 for the 2-butanone ion, at 10 eV ionizing electron energy, the ratio $(M–CH_3)/(M–R)$ for methyl ketone ions increases in proportion to the difference between the appearance energies (AEs) of the fragments, and AE(–R) increases with increasing size of R, the larger alkyl lost. In Rice–Ramsperger–Kassel–Marcus (RRKM) theory, rates at low energies are established primarily by critical energies, and rates at high energies are determined by transition state "tightness" or "looseness" (values of frequencies for transition state vibrations and the number of internal rotations). This predicts that in the absence of other factors the lower threshold processes, i.e., the loss of the smaller alkyl, should be favored at all energies [15], in contrast to the actual patterns. One explanation proposed for the inversion of the relative abundances of α-cleavage products on going from low to high energy is that abundances of the larger α-cleavage products are reduced by further dissociation at high energies [11]. However, this hypothesis clearly does not always apply [12,15]. Other suggested explanations are that rearrangements only at low internal energies or reactions from excited electronic states cause the switch [12]. However, while they occur, dissociations from isolated electronic states of ions are unusual [16]. Prior rearrangements may influence some [17–21] but not all of the dissociations studied. Thus, why the losses of larger alkyls increase more rapidly in rate with increasing internal energy than do those of smaller ones has long been one of the mysteries of gas phase ion chemistry.

We recently combined ab initio transition state energies and vibrational frequencies with RRKM theory to elucidate why methane is lost much more abundantly than $H^{\bullet}$ from the propane ion [22], despite the former process having a slightly higher critical energy and expectations that its transition state would be much "tighter". Substantial decreases in the values of a number of vibrational frequencies in the transition state for the rate-determining step in methane elimination, CC bond-breaking vs. no substantial changes in transition state frequencies for the loss of $H^{\bullet}$ proved to be the cause of this surprising pattern of increases in rate with energy in these reactions. This suggested the hypothesis investigated here—that greater decreases in transition state frequencies also cause the rates of loss of large alkyls to increase more rapidly than those of small alkyls with increasing energy in the dissociating ion. Other studies have attributed the slower rates of $H^{\bullet}$ than alkyl losses to centrifugal barriers [23], transition state switching and differences in the values of the rotational constants for the transition states [24,25], effects of the rotational

energy [26], and most recently, the occurrence of minimum entropy transition states well below the actual dissociation thresholds [27].

To clarify the origins of the effect of neutral fragment size on the dependence of dissociation rate on ion internal energy, we used RRKM theory to explore what determines the dependence on internal energy of the relative rates of $H^{\bullet}$, $CH_3^{\bullet}$ and $C_2H_5^{\bullet}$ losses from appropriate ions. In this work, RRKM calculations were carried out using combinations of photoionization appearance energies (PIAEs), theoretical energies and vibrational frequencies and thresholds for ion–neutral complex formation based on the AEs for alkane eliminations. Low energy alkane eliminations from such complexes are direct evidence that associated alkyl losses may have transition states below their dissociation thresholds. Consistent with this, entropy bottlenecks (points of minimum densities of states) below the threshold for full dissociation on the reaction coordinate by simple bond cleavages can quickly become rate determining transition states as the energy in a system rises beyond the dissociation threshold [25,28]. Vibrational frequencies, ground state energies and transition state energies were obtained by hybrid functional B3LYP/6-31G(d) and B3LYP/6-311G(d,p) theories [29,30]. For convenience, these theories will hereafter be referred to as DFT.

2. Results and discussion

Rearrangements in *n*-propyl, *n*-butyl and longer chains can lead to loss of alkyl groups from the ends of longer alkyl chains such that alkyl losses by other mechanisms compete with α-cleavages [17–21]. Therefore, we confined our studies to the losses of $H^{\bullet}$, $CH_3^{\bullet}$ and $C_2H_5^{\bullet}$ by unequivocal α-cleavages.

2.1. Experimental observations

Fragmentation patterns, PIAEs and combined product heats of formation are given in Table 1. The extent of a given reaction at a particular energy is proportional to the first differential of the photoionization efficiency (FDPI) curve at that energy [31,32]. Therefore, FDPI curves were recorded for each fragmentation studied to obtain the dependence of its rate on the internal energy of the dissociating ion.

2.1.1. $CH_3CH_2OH^{\bullet+}$

The following dissociations of $CH_3CH_2OH^{\bullet+}$ were examined (Scheme 1). AEs in Table 1 place the threshold for $CH_3^{\bullet}$ loss from $CH_3CH_2OH^{\bullet+}$ 45 kJ mol^{-1} above that for the loss of $H^{\bullet}$. Dissociation energies derived by subtracting the ionization energy from the AEs are 10 and 14 kJ mol^{-1} lower than corresponding differences between published 298 K heats of formation (Table 1). For simple cleavages, most such differences throughout this work are substantially diminished (from an average of -13.6 ± 6.6 to 4.6 ± 7.0 kJ mol^{-1}) by using the formula $\Delta_f H^{\circ}_{298}(A^+) = AE(A^+)_{298} + \Delta_f H^{\circ}_{298}(AB) - \Delta_f H^{\circ}_{298}(B) + \Delta H_{corr}$ [33] to correct for the thermal energy of the fragments at the non-equilibrium temperature at which they are formed at threshold upon photoionization. The several differences that remain may reflect effects of some excess energy stemming from kinetic/competitive shifts on AEs. The generally quite good agreement between corrected PI thresholds and values predicted from published data (Table 1) demonstrate the general accuracy of the PIAEs.

Despite its 45 kJ mol^{-1} higher onset, $CH_3^{\bullet}$ loss is about twice as abundant as is $H^{\bullet}$ loss in the 70 eV mass spectrum of ethanol (Table 1). The loss of $H^{\bullet}$ necessarily dominates between its threshold and the threshold for the loss of $CH_3^{\bullet}$, as seen in the FDPI curves for the losses of $H^{\bullet}$ and $CH_3^{\bullet}$ in Fig. 1. However, the loss of $CH_3^{\bullet}$ becomes more abundant than loss of $H^{\bullet}$ at just 10 kJ mol^{-1} above the onset for the former fragmentation. As in the normal mass spectrum, $CH_3^{\bullet}$ loss is about twice as abundant as is the loss of $H^{\bullet}$ in the high energy region of the FDPI curves. Further dissociation did not affect these relative abundances, as it requires more than 240 kJ mol^{-1} to dissociate $CH_3CH{=}OH^+$ [34], and even more energy to dissociate $CH_2{=}OH^+$ [35]. Thus, despite its having a substantially higher onset, $CH_3^{\bullet}$

Table 1
Product abundances, thermochemical data and photoionization appearance energies

Compound	Relative abundance[a]	$\Delta_f H$[b] (kJ mol^{-1})	$\Delta\Delta_f H$[c] (kJ mol^{-1})	PI AE[d] (eV)	ΔPI AE (kJ mol^{-1})	ΔH_{corr} (kJ mol^{-1})	ΔH_{corr} + ΔPI AE
Ethanol							
CH_2=OH^+ + $CH_3^\bullet$	100	855	80	11.19	70	14.4	84
CH_3CH=OH^+ + $H^\bullet$	49	814	39	10.73	25	13.2	38
$CH_3CH_2OH^{\bullet+}$	23	775	0	10.47			
2-Propanol							
CH_3CH=OH^+ + $CH_3^\bullet$	100	742	38	10.32	19	17.4	36
CH_2=$CHOH^{\bullet+}$ + CH_4	3.0	696	−8	10.19	7	16.1	23
CH_3C(=OH^+)CH_3 + $H^\bullet$	3.5	708	4	10.13	1	19.4	20
$CH_3CH(OH^{\bullet+})CH_3$	0.3	704	0	10.12			
2-Butanol							
CH_3CH=OH^+ + $C_2H_5^\bullet$	100	715	54	10.25	35	20.0	55
CH_2=$CHOH^{\bullet+}$ + C_2H_6	8.3	687	26	10.05	15	17.9	33
CH_3CH_2CH=OH^+ + $CH_3^\bullet$	20	696	35	10.16	26	20.7	47
CH_3CH=$CHOH^+$ + CH_4	0.6	602	−59	10.02	12	20.1	32
CH_3C(=OH^+)CH_2CH_3 + $H^\bullet$	1.3	673	12	∼9.9		20.3	
$CH_3CH(OH^{\bullet+})CH_2CH_3$	0.3	661	0	9.89			
2-Methylpropane							
$CH_3CH^+CH_3$ + $CH_3^\bullet$	100	948	63	11.01	43	19.7	62
CH_3CH=$CH_2^{\bullet+}$ + CH_4	34	884	−1	10.79[e]	22	18.5	40
$(CH_3)_3C^+$ + $H^\bullet$	3.0	929	44	10.82	25	19.5	45
$CH_3CH(CH_3)CH_3^{\bullet+}$	2.8	885	0	10.56			
2-Butanone							
CH_3CO^+ + $C_2H_5^\bullet$	100	775	88	10.40	84	18.8	103
$CH_3CH_2CO^+$ + $CH_3^\bullet$	6.1	764	83	10.20	64	19.4	83.4
$CH_3C(O^{\bullet+})C_2H_5$	16	681	0	9.53			

[a] From Stenhagen et al. [46]. At 70 eV electron energy.
[b] Based on values given in Table 3.
[c] $\sum \Delta_f H$(products) − $\Delta_f H$(molecular ion) from the preceding column.
[d] This work.
[e] Value uncertain.

loss surpasses $H^\bullet$ loss at higher ion internal energies, suiting the dissociations of the ethanol ion to this study.

2.1.2. $CH_3CH(OH^{\bullet+})CH_3$

We examined the following dissociations of the 2-propanol ion (Scheme 2). Alkane eliminations from

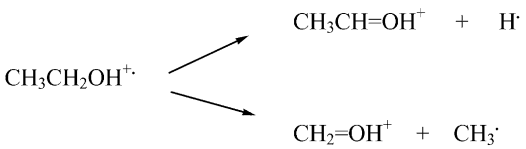

Scheme 1.

secondary alcohol ions give primarily enol products [36,37], as depicted. As for $CH_3CH_2OH^{\bullet+}$, the loss of $H^\bullet$ has the lower measured onset—18 kJ mol^{-1} below that for loss of $CH_3^\bullet$.

$C_2H_5O^+$ is 33 times more abundant than $C_3H_7O^+$ in the 70 eV mass spectrum of 2-propanol (Table 1), and above its onset the FDPI curve for the former rises about 15 times more rapidly with increasing internal energy than does that of the latter (Fig. 2). Further dissociation of the product CH_3C(=OH^+)CH_3 does not influence its FDPI abundance, as at least 242 kJ mol^{-1} is required to dissociate that ion [38]. Thus, the loss of $H^\bullet$ from the 2-propanol ion is even less competitive with loss of $CH_3^\bullet$ than it is in the dissociations

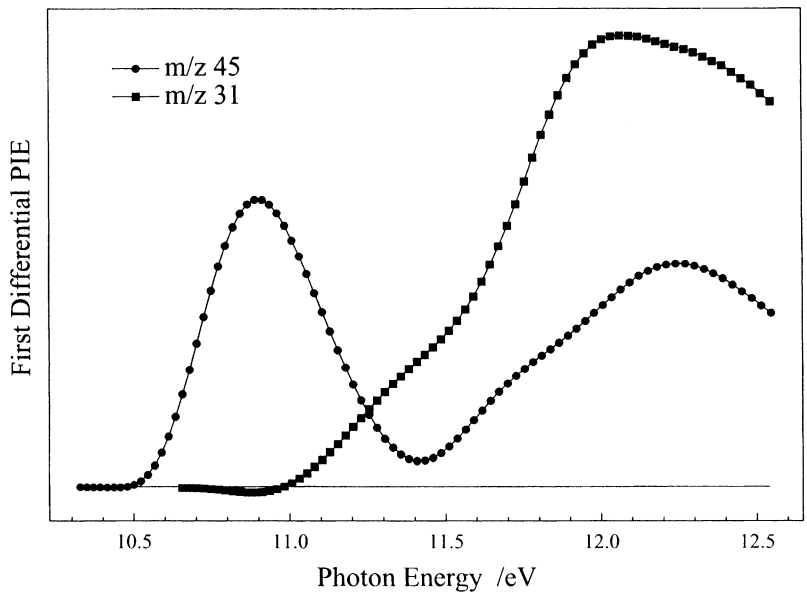

Fig. 1. FDPI curves for the losses of $H^{\bullet}$ (m/z 45) and $CH_3^{\bullet}$ (m/z 31) from $CH_3CH_2OH^{\bullet+}$. These plots give the relative abundances of the two processes as a function of ion internal energy, an energy which is coincident with the photon energy on the X-axis minus the ionization energy. Note that $H^{\bullet}$ loss has the lowest threshold, but that the $CH_3^{\bullet}$ loss becomes dominant at higher energies.

of $CH_3CH_2OH^{\bullet+}$. The smaller difference between the appearance energies of the products in comparison to the corresponding difference for the ethanol ion (18 kJ mol^{-1} vs. 45 kJ mol^{-1} for $CH_3CH_2OH^{\bullet+}$) is one factor that reduces the relative abundance of $H^{\bullet}$ loss. The lower threshold for loss of $H^{\bullet}$ than for loss of $CH_3^{\bullet}$ should compel the former process to be more important than the latter below the threshold for the latter. That it is not (Fig. 2) is attributable to suppression of $H^{\bullet}$ loss by the competing loss of CH_4, a process

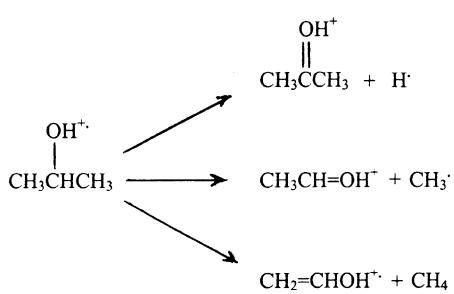

Scheme 2.

$CH_3CH_2OH^{\bullet+}$ does not undergo. (The tail for $CH_3^{\bullet}$ loss below its threshold reflects the thermal content of 2-propanol.) Even near threshold, methane is lost several times as often as is $H^{\bullet}$, despite the expectation that the elimination would have a much more highly ordered transition state. This adds another example of an alkane elimination being faster than a competing $H^{\bullet}$ loss to that of the propane ion [22]. As we have described previously, we attribute this to alkane eliminations being two step reactions (Scheme 3), the first a fast, rate-determining bond cleavage [6,39].

According to this rationalization, even below the threshold for simple dissociation of the complex, CC bond cleavage to form an ion–neutral complex is much faster than CH bond cleavage, thus, causing alkane elimination to be more rapid than $H^{\bullet}$ loss, in contrast to what would be the case if the rate-determining transition state for methane elimination were highly ordered. Furthermore, according to this model, the threshold for alkane elimination is the upper limit for the onset for complex formation.

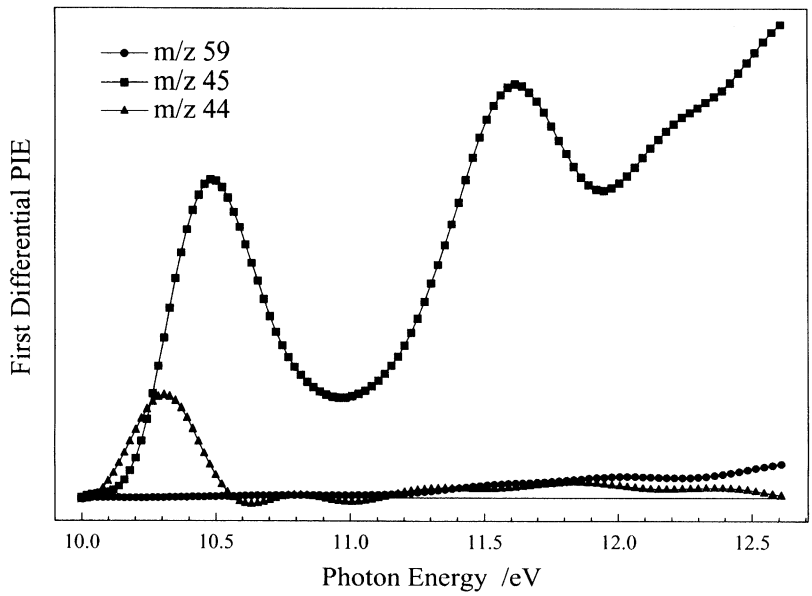

Fig. 2. FDPI curves for the losses of $H^{\bullet}$ (*m*/*z* 59), $CH_3^{\bullet}$ (*m*/*z* 45) and CH_4 (*m*/*z* 44) from $CH_3CH(OH^{\bullet+})CH_3$. Note that there are only $H^{\bullet}$ and CH_4 losses near threshold, but that the $CH_3^{\bullet}$ loss rapidly becomes dominant with increasing energy.

2.1.3. $CH_3CH(OH^{\bullet+})C_2H_5$

The 2-butanol ion loses $C_2H_5^{\bullet}$, $CH_3^{\bullet}$ and $H^{\bullet}$ (Scheme 4), providing a system for characterizing competition between losses of different sized alkyl groups as well as between alkyl fragments and $H^{\bullet}$ loss.

As expected, for the 2-butanol ion AEs, combined product heats of formation and the abundances of the corresponding products in the 70 eV mass spectrum (Table 1) are in the order $-H^{\bullet} < -CH_3^{\bullet} < -C_2H_5^{\bullet}$. Appearance energies measured here for dissociations of the 2-butanol ion are within 0.00–0.05 eV of ones measured previously by photoelectron–photoion coincidence measurements [40]. Rates of bond cleavage as a function of internal energy also increase in the order $-H^{\bullet} < -CH_3^{\bullet} < -C_2H_5^{\bullet}$ (FDPI curves, Fig. 3). Thus, for simple cleavages, the threshold and the rapidity of the increase in the dissociation rate with increasing internal energy both are highest for the loss of the largest neutral fragment. Furthermore, $C_2H_5^{\bullet}$ loss is less abundant than $CH_3^{\bullet}$ loss very near threshold (Fig. 3a), so the rates of these dissociations display the

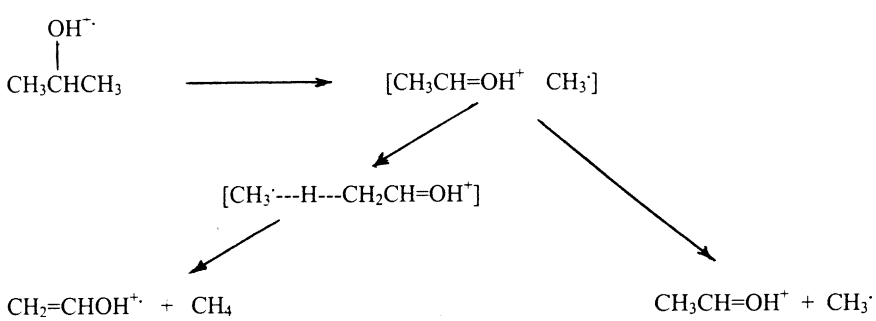

Scheme 3.

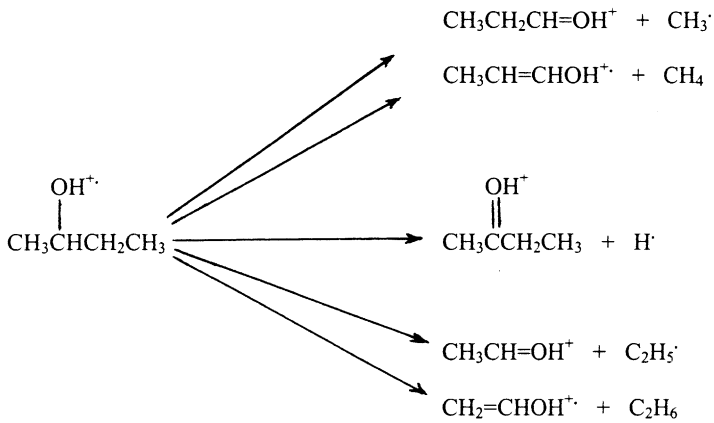

Scheme 4.

crossover in abundances of alkyl losses with increasing energy that we set out to address. Further dissociation did not significantly influence the FDPI abundance of $C_2H_5CH{=}OH^+$, as it takes 167 kJ mol^{-1} to dissociate that ion [38]. Even more energy is required to dissociate the other product ions (see above), so further dissociations did not significantly affect the PI results presented.

Methane is lost from the 2-butanol ion more abundantly at low energies than is H$^\bullet$. However, ethane elimination strongly dominates both of these reactions for about 100 kJ mol^{-1} above threshold (Fig. 3a). These results together with those for dissociations of $CH_3CH(OH^{\bullet+})CH_3$ (above) and $(CH_3)_3CH^{\bullet+}$ (below) establish that most alkane eliminations are faster than competing H$^\bullet$ losses.

Assuming that, as described above, both alkyl and corresponding alkane losses involve similar cleavage of the same CC bond, comparing the summed $-CH_3^\bullet$ and $-CH_4$ to the $-C_2H_5^\bullet$ plus $-C_2H_6$ curves (Fig. 3b) leads to the conclusion that cleavage of the CC bond to $C_2H_5^\bullet$ is faster than cleavage of bonds to CH_3 and H down to below the thresholds for the complete dissociations. Thus, even below the onset of separation of the fragments, bond cleavage in the 2-butanol ion is favored in the order C–C_2H_5 > C–CH_3 > C–H. This probably reflects stronger ion-induced dipole attractions between $CH_3CH{=}OH^+$ and $C_2H_5^\bullet$ than between $C_2H_5CH{=}OH^+$ and $CH_3^\bullet$ because, if ion-induced dipole attractions are stronger, covalent attractions would be weaker and the transition state looser at the same total binding energy. Stronger non-covalent attraction between small ion–large neutral partners in complexes has been proposed to explain a general preference for losses of larger alkanes in dissociations of small radical cations [41,42]. More substantial ion-noncovalent attractions to larger R groups is also supported by the substantially lengthened CC distances to the longer alkyl groups in the ground state 2-butanol and 2-butanone ions in DFT theory presented below. Thus "size effects" favoring eliminations of larger alkanes at low energies and loss of larger alkyls at high energies apparently have a common origin in looser bonds to larger alkyl groups.

2.1.4. $(CH_3)_3CH^{\bullet+}$

FDPI curves (Fig. 4) were determined for the losses of $CH_3^\bullet$, CH_4 and H$^\bullet$ from the 2-methylpropane ion (Scheme 5). The losses of $CH_3^\bullet$ and CH_4 from this ion were previously studied by photoionization [43], photoelectron–photoion coincidence [44] and ab initio [45] methods.

Paralleling observations described above, the total product heats of formation, the threshold, the FDPI abundance and the 70 eV abundance of $CH_3^\bullet$ loss were all appreciably higher than corresponding values for H$^\bullet$ losses. Therefore, this system is yet another example of an alkyl loss being strongly favored

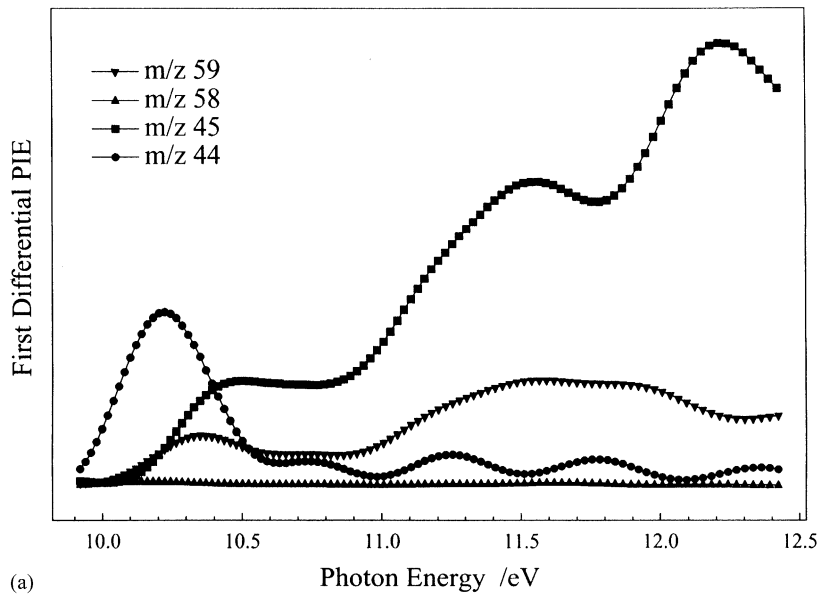

(a)

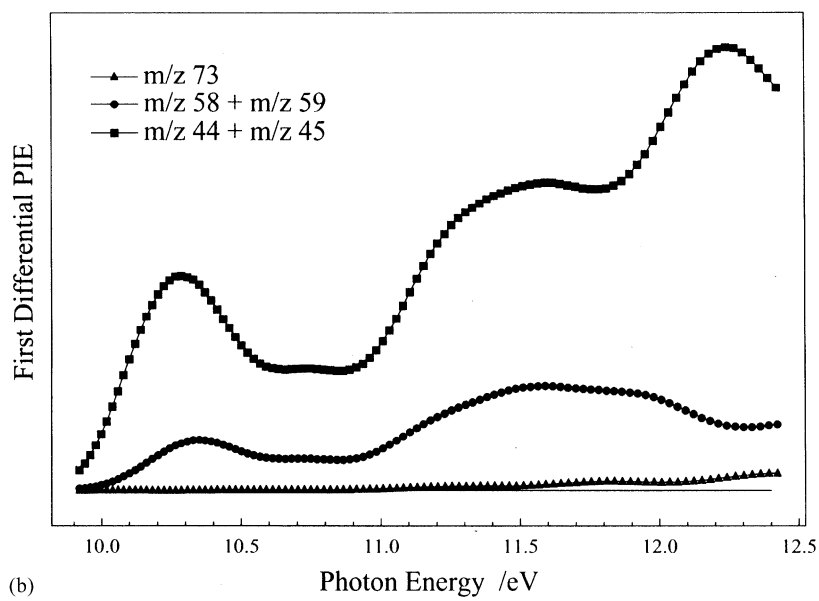

(b)

Fig. 3. (a) FDPI curves for the losses of $CH_3^{\bullet}$ (*m*/*z* 59), CH_4 (*m*/*z* 58), $C_2H_5^{\bullet}$ (*m*/*z* 45) and C_2H_6 (*m*/*z* 44). Note the dominance of ethane elimination at low energies, demonstrating that cleavage of the C–CH_2CH_3 bond is strongly preferred even very near threshold; (b) FDPI curves for the losses of $H^{\bullet}$ (*m*/*z* 73) and the combinations $CH_3^{\bullet}$ (*m*/*z* 59) plus CH_4 (*m*/*z* 58) and $C_2H_5^{\bullet}$ (*m*/*z* 45) plus C_2H_6 (*m*/*z* 44) from $CH_3CH(OH^{\bullet+})CH_2CH_3$. Note the order of preferred bond cleavage implied by the data: C–CH_2CH_3 > C–CH_3 > C–H.

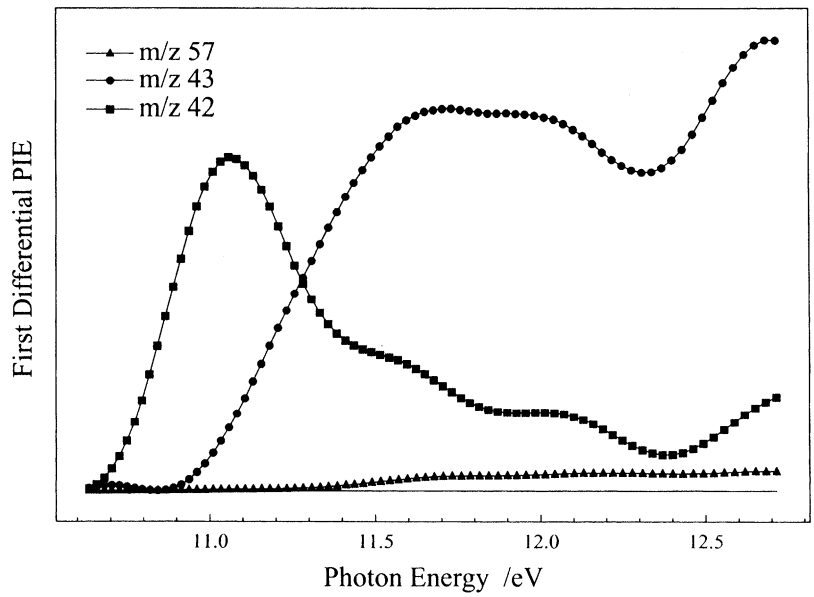

Fig. 4. FDPI curve for the losses of $H^{\bullet}$ (*m*/*z* 57), $CH_3^{\bullet}$ (*m*/*z* 43) and CH_4 (*m*/*z* 42) from $CH_3CH(CH_3)CH_3^{\bullet+}$. Note that there is only $H^{\bullet}$ and CH_4 loss near threshold, but that the $CH_3^{\bullet}$ loss becomes most important at higher energies.

over $H^{\bullet}$ loss despite the latter being energetically favored, establishing the generality of this pattern in dissociations of radical cations. Even near its threshold the relative abundance of the $H^{\bullet}$ loss was quite low, undoubtedly due to strong competition from the elimination of methane in that energy region.

2.1.5. $CH_3C(\equiv O^{\bullet+})C_2H_5$

The dissociations of the 2-butanone radical cation (Scheme 6) were characterized to compare the losses of two alkyl fragments of different size in the absence of competing $H^{\bullet}$ loss and alkane eliminations.

As for the 2-butanol ion, AE(–$CH_3^{\bullet}$) is lower than AE(–$C_2H_5^{\bullet}$), but the product of the latter dissociation is 17 times more abundant in the 70 eV mass spectrum (Table 1). In the FDPI curves, the loss of $C_2H_5^{\bullet}$ did not surpass the loss of $CH_3^{\bullet}$ until ca. 200 kJ mol^{-1} above threshold (Fig. 5), a point at which the abundance of the product of $CH_3^{\bullet}$ loss decreased substantially. This occurs at approximately the energy at which dissociation of $C_2H_5CO^+$ to $C_2H_5^+ + CO$ becomes feasible (Fig. 5), suggesting that in this case, further dissociation influences the relative abundances of the primary products at high energies. An abundant $C_2H_5^+$ in the mass spectrum of 2-butanone is consistent with this. Nonetheless, the sum of the abundances of $C_2H_5^+$ and $C_2H_5CO^+$ in the 70 eV mass spectrum of that substance is only 28% of that of $CH_3CO^+ + CH_3^+$, so the upper limit to the $-CH_3^{\bullet}/-C_2H_5^{\bullet}$ ratio is

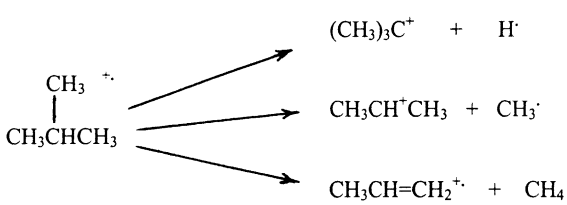

Scheme 5.

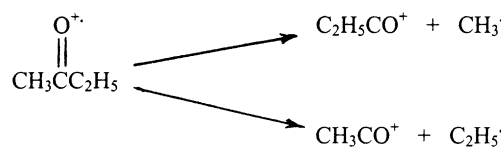

Scheme 6.

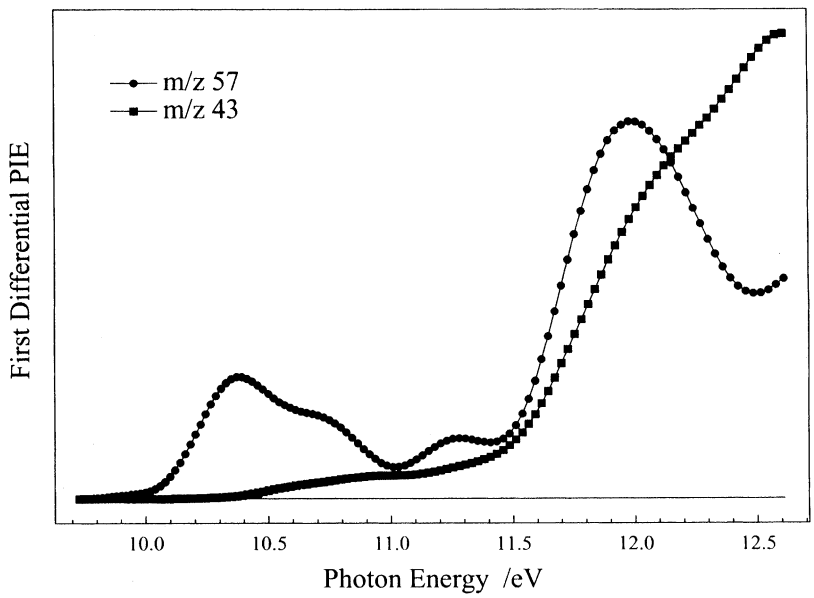

Fig. 5. FDPI curves for the losses of $CH_3^{\bullet}$ (*m/z* 57) and $C_2H_5^{\bullet}$ (*m/z* 43) from the 2-butanone ion. Note that methyl loss dominates near threshold, but that the $C_2H_5^{\bullet}$ loss becomes more important at higher energies.

0.28. Thus, even if all alkyl ions were formed by two consecutive dissociations, adding their abundances to the acyl abundances would still leave loss of the larger alkyl several fold favored at higher energies. Alkyl ions may be formed from $CH_3C(=O^{\bullet+})CH_2CH_3$ in part by direct dissociation to those ions plus acyl radicals, pathways energetically favored over two consecutive dissociations to CH_3^+ and $C_2H_5^+$. However, dissociation of the 2-butanone ion directly to CH_3^+ and $C_2H_5^+$ would violate the Stevenson–Audier rule, which states that ions dissociate such that the charge goes to form the energetically favored set of products [47,48]. It is unclear whether such a violation occurs in the formation of CH_3^+ from the acetone ion [49], so the importance of direct dissociation to alkyl ions in the dissociations of the 2-butanone ion is also uncertain.

3. DFT theory

We used theory to seek insight into why bonds to larger groups cleave preferentially in ions in the gas phase, in particular to try to establish whether changes in vibrational frequencies in the transition states cause losses of larger fragments to have faster rates. B3LYP/6-31G(d) and B3LYP/6-311G(d,p) theories were used (Table 2) to obtain transition state energies and dissociation thresholds; vibrational frequencies were obtained by B3LYP/6-31G(d) theory. Relevant product heats of formation were obtained from the literature (Table 3). Theoretical studies of the 2-methylpropane ion are not reported due to failure to find a transition state for $H^{\bullet}$ loss from that ion, despite substantial effort to do so. However, calculating energies at different CH bond lengths for that reaction suggested an energy maximum, i.e., transition state, around 2.2 Å. No search was made for a transition state for $CH_3^{\bullet}$ loss from the 2-methylpropane ion.

One lengthened CC bond (Table 4) and associated lowered energies relative to those of the ion at the geometry of the neutral (Table 5) were observed for all molecular ions. Agreement (see following sections) between DFT results for ground state species corrected for Franck–Condon effects and PI dissociation energies corrected to 0 K [33] was better than

Table 2
Hybrid functional theory energies for stationary points

Compound	Fragments	$\Delta\Delta_f H$ (kJ mol^{-1})[a]	Ab initio ($\Delta\Delta_f H$)[b] (kJ mol^{-1})		Ab initio (TS)[c] (kJ mol^{-1})	
Ethanol	CH_2=OH^+ + $CH_3^\bullet$	80	109	96	83	72
	CH_3CH=OH^+ + $H^\bullet$	39	67	64	65	63
	$CH_3CH_2OH^{\bullet+}$	0				
2-Propanol	CH_3CH=OH^+ + $CH_3^\bullet$	38	49	37	44	33
	CH_3C(=OH^+)CH_3 + $H^\bullet$	4	38	36	50	48
	$CH_3CH(OH^{\bullet+})CH_3$	0				
2-Butanol	CH_3CH=OH^+ + $C_2H_5^\bullet$	54	79	68	56	47
	CH_3CH_2CH=OH^+ + $CH_3^\bullet$	35	80	70	–[d]	–[d]
	CH_3C(=OH^+)CH_2CH_3 + $H^\bullet$	12			82	74
	$CH_3CH(OH^+)CH_2CH_3$	0				
2-Butanone	CH_3CO^+ + $^\bullet C_2H_5$	88	111	98	103	92
	$CH_3CH_2CO^+$ + $CH_3^\bullet$	83	110	98	108	97[d]
	$CH_3C(O^{\bullet+})C_2H_5$	0				

[a] Difference between product heat of formation and the heat of formation of the ionized molecule from values in Table 3.

[b] Energies required according to theory to form the products; values in the first column were derived from B3LYP/6-31G(d) and B3LYP/6-31G(d) theory, values in the second columns are from B3LYP/6-311G(d,p) and B3LYP/6-311G(d,p) theory.

[c] Energies required to reach transition states: first column—by B3LYP/6-31G(d) and B3LYP/6-31G(d) theory; second column—by B3LYP/6-311G(d,p) and B3LYP/6-311G(d,p) theory.

[d] Optimization at the B3LYP/6-311G(d,p) was not achieved for this transition state; the number is the B3LYP/6-311G(d,p) and B3LYP/6-31G(d) value.

without such corrections for most reactions treated, supporting the reasonableness of the energies and geometries for stable species derived by DFT. However, it should be noted that photon ionization energies are typically lower than vertical ionization energies, so the Franck–Condon corrections derived from theory are probably overestimations.

3.1. $CH_3CH_2OH^{\bullet+}$

At both levels of DFT, a transition state with motion directed primarily along the CC bond was found for $CH_3^\bullet$ loss from $CH_3CH_2OH^{\bullet+}$ at about 25 kJ mol^{-1} below the combined DFT heats of formation of the separated products. However, this transition state might not really exist, as we were unable to find it with QCISD/6-31G(d) theory starting the search from the B3LYP/6-31G(d) transition state geometry, even though evidence was obtained by QCISD/6-31G(d) theory for a transition state between a CC bond length of 5.0 and 5.1 Å. However, this transition state differed from the B3LYP transition state in that the primary motion was an angular movement of the methyl, presumably to form a [$CH_3^\bullet$ CH_2OH^+] complex, rather than a CC extension. In being 24–26 kJ mol^{-1} below its dissociation products, the DFT transition state for $CH_3^\bullet$ loss resembles the transition state expected for forming the ion–neutral complex [$CH_3^\bullet$ CH_2=OH^+] [6,41,42] and the tight (early) transition states postulated by transition state switching (TSST) [25,50] and variational transition state theories [28]. As will be described, energies of transition states located by DFT were below those of the dissociated products for most of the other alkyl losses that we studied. However, RRKM calculations (see below) indicate that tight TSST transition states and the DFT transition states do not coincide.

The CC bond is elongated to 5.26 Å at the DFT transition state for $CH_3^\bullet$ loss (Table 4), a distance at which the CC bond is effectively broken. The energy of this transition state is about 25 kJ mol^{-1} below the energy of the fully dissociated products. Location of the transition state close to the threshold for dissociation of the fragments is supported by the marked lowering

Table 3
Heats of formation (kJ mol^{-1}) used for product heats of formation and thermochemical thresholds in Tables 1 and 2

CH_2=OH^+	709[a]	$CH_3^\bullet$	146[b]
CH_3CH=OH^+	596[c]	$H^\bullet$	218[b]
$CH_3CH_2OH^{\bullet+}$	775[d]	CH_3CH_2OH	−235[b]
CH_2=$CHOH^{\bullet+}$	771[e]	CH_4	−75[b]
$CH_3C(=OH^+)CH_3$	490[f]	C_2H_6	−84[b]
$CH_3CH(OH^{\bullet+})CH_3$	704[d]	$CH_3CH(OH)CH_3$	−273[b]
CH_3CH_2CH=OH^+	550[f]	$CH_3CH_2^\bullet$	119[b]
CH_3CH=$CHOH^+$	677[g]		
$CH_3C(=OH^+)CH_2CH_3$	455[f]		
$CH_3CH(OH^{\bullet+})CH_2CH_3$	661[d]	$CH_3CH(OH)CH_2CH_3$	−293[b]
$CH_3CH^+CH_3$	802[a]		
CH_3CH=$CH_2^{\bullet+}$	959[f]		
$(CH_3)_3C^+$	711[a]		
$CH_3CH(CH_3)CH_3^{\bullet+}$	885[d]	$CH_3CH(CH_3)CH_3$	−134[b]
CH_3CO^+	656[a]		
$CH_3CH_2CO^+$	618[h]		
$CH_3C(=O^{\bullet+})C_2H_5$	681[d]	$CH_3C(=O)C_2H_5$	−239[b]

[a] From [64].
[b] http://webbook.nist.gov, February 2000.
[c] From [65].
[d] Based on the corresponding PI ionization potential in Table 1 and $\Delta_f H$(neutral) in this table.
[e] From [66].
[f] From [67].
[g] From [68].
[h] Based on AE($C_2H_5CO^+$) from 2-butanone (Table 1, this work) and $\Delta_f H$(2-butanone) in this table. Also see [69].

of five vibrational frequencies in the transition state relative to their values in the ground state ion (Table 6). Transition states for formation of complexes occur below the energy required to completely separate the fragments as bonds become stretched sufficiently to permit rotation of the fragments perpendicularly to the breaking bond [51]. The energy of the DFT transition state, its lowered frequencies and the general tendency to form complexes starting below the threshold for dissociation by CC cleavage suggest that a transition state below the threshold for complete simple dissociation controls the rate of $CH_3^\bullet$ loss from $CH_3CH_2OH^{\bullet+}$. It is important to note, however, that this may be a minimum entropy transition state that need not coincide with the DFT transition state located based on the one imaginary frequency criterion. RRKM calculations presented in the next section do suggest that the rate-determining transition states are earlier than the DFT transition states found for alkyl loss.

A transition state was found for $H^\bullet$ loss at about 1 kJ mol^{-1} below the energy of the separated products with the CH bond stretched to about twice its normal length (Table 4). This presumably reflects weaker noncovalent attractions in [CH_3CH=OH^+ $H^\bullet$] than in [$CH_3^\bullet$ CH_2=OH^+]. A transition state for $H^\bullet$ loss was also located by QCISD/6-31G(d) theory 54.7 kJ mol^{-1} above the ground state of $CH_3CH_2OH^{\bullet+}$, supporting the reality of that transition state. The vibrational frequencies in this transition state were quite similar to those of the ground state ion.

Both levels of DFT gave substantially greater differences between the product and reactant energies than did the PI measurements. This is attributable to the stabilization of the DFT ground state ion upon lengthening of the CC bond from 1.536 Å in the neutral to 1.742 Å in the ion. Photoionization would generate the ion initially in the geometry of the neutral due to the Franck–Condon effect. The long-bonded ground

Table 4
B3LYP/6-31G(d,p) bond lengths (Å) at stationary points

	CC	CH
Ethanol		
Neutral	1.5363	1.1026, 1.0950
Ion	1.7422	1.0920, 1.0907
Transition state	5.2627	2.1364
2-Propanol		
Neutral	1.5239	1.1039
Ion	1.8069	1.0963
Transition state	5.8254	1.8746
2-Butanol		
Neutral	1.5300[a], 1.5294[b]	1.1048
Ion	1.4936[a], 1.9562[b]	1.0963
Transition state	5.2602[b]	1.8718
	C–CH_3	C–CH_2CH_3
2-Butanone		
Neutral	1.5209	1.5256
Ion	1.5149	1.5866
Transition state	8.3854	5.3354

[a] C–CH_3.
[b] C–CH_2CH_3.

state of $CH_3CH_2OH^{\bullet+}$ was 34 kJ mol^{-1} more stable than was $CH_3CH_2OH^{\bullet+}$ at the geometry of the neutral molecule. Gauld and Radom found an extended CC bond in $CH_3CH_2OH^{\bullet+}$ by B3LYP/6-31G(d) and 20 higher levels of theory [52], supporting its reality. Adding 34 kJ mol^{-1} to the PI dissociation energies removes the difference between energies derived by experiment and those obtained by theory (Table 5). Marked CC bond lengthening (Table 4) and the associated decrease in precursor ion energy nicely account for the differences between experimental and theoretical threshold energies that occur throughout this work (Table 2), evidence that the long bonds observed by theory are the source of those discrepancies. Consistent with present results, previous ab initio studies revealing long-bonded ions have also given theoretical ionization potentials significantly lower than experimental ones [53,54].

3.2. $CH_3CH(OH^{\bullet+})CH_3$

A transition state for CC bond-breaking in $CH_3CH(OH^{\bullet+})CH_3$ was found by DFT theory 4–5 kJ mol^{-1}

Table 5
Effects of long-bond formation on ground state and dissociation energies

Compound	ΔAE	ΔH_{corr}[a]	ΔAE (0 K) (kJ mol^{-1})	FC_{corr}[b] (kJ mol^{-1})	ΔAE + FC_{corr} (kJ mol^{-1})	ΔDFT[c,d] (kJ mol^{-1})
Ethanol						
CH_2=OH^+ + $CH_3^{\bullet}$	70	7.5	78	34	112	109
CH_3CH=OH^+ + $H^{\bullet}$	25	7.5	32	34	66	67
2-Propanol						
CH_3CH=OH^+ + $CH_3^{\bullet}$	19	10.3	29	40	69	49
$CH_3C(=OH^+)CH_3$ + $H^{\bullet}$	1	10.3	11	40	51	38
2-Butanol						
CH_3CH=OH^+ + $C_2H_5^{\bullet}$	35	14.0	49	70	119	79
CH_3CH_2CH=OH^+ + $CH_3^{\bullet}$	26	14.0	40	70	110	80
2-Butanone						
CH_3CO^+ + $C_2H_5^{\bullet}$	84	13.6	98	14	112	111
$C_2H_5CO^+$ + $CH_3^{\bullet}$	64	13.6	78	14	92	110

[a] The correction used to convert the measured PIAEs to the values they would have if measured at 0 K. This is the enthalpy at 298 K—the enthalpy at 0 K minus 5/2*RT*. These enthalpy differences were obtained using the Gaussian programs [59]. This conversion is made for comparing experiment and theory because theory gives 0 K enthalpies.

[b] The difference between the optimized DFT energy of the precursor ions and the DFT energy of the ions in the geometry of the corresponding neutral molecules.

[c] The DFT energies required to dissociate each precursor ion to the indicated products.

[d] These DFT dissociation energies are on average 28.5 ± 8.5 kJ mol^{-1} (±S.D.) higher than the 0 K ΔAEs and 11 ± 19 kJ mol^{-1} lower than the ΔAE + FC_{corr} values. The former difference is significant ($P < 0.001$, paired *t*-test), but the latter is not.

Table 6
Values of the six lowest B3LYP/6-31G(d) and B3LYP/6-31G(d) frequencies[a] for ground and transition states

$CH_3CH_2OH^{\bullet+}$								
Ground state	224	285	386	509	826	853		
$CH_3CH{=}OH^+ + H^\bullet$	189	356	369	468	644	885		
$CH_2{=}OH^+ + CH_3^\bullet$	15	60	72	108	109	769		
$CH_3CHOH^{\bullet+}CH_3$								
Ground state	169	220	273	304	428	444		
$CH_3C(=OH^+)CH_3 + H^\bullet$	162	198	362	431	480	497		
$CH_3CH{=}OH^+ + CH_3^\bullet$	15	21	25	95	99	139		
$CH_3CHOH^{\bullet+}CH_2CH_3$								
Ground state	85	186	197	215	247	300		
$CH_3C(=OH^+)C_2H_5 + H^\bullet$	79	164	205	239	377	434		
$C_2H_5CH{=}OH^+ + CH_3^\bullet$	–	–	–	–	–	–		
$CH_3CH{=}OH^+ + C_2H_5^\bullet$	12	21	30	41	61	119		
$CH_3C(=O^{\bullet+})CH_2CH_3$								
Ground state	63	102	207	232	339	372	515	578
$C_2H_5CO^+ + CH_3^\bullet$	9.6	15	25	72	75	178	190	388
$CH_3CO^+ + C_2H_5^\bullet$	15	27	29	37	63	160	223	298

[a]These frequencies were scaled by multiplication by 0.9806, the scaling factor for B3LYP/6-31G(d) and B3LYP/6-31G(d) theory. Scott and Radom [63].

below the corresponding dissociation products (Table 2). A transition state was found for loss of $H^\bullet$ by both levels of DFT 12 kJ mol^{-1} above the DFT energy of the corresponding products, somewhat exceeding the corresponding PI difference of only 1 kJ mol^{-1}, and a published $\Delta_f H$(products) − $\Delta_f H(CH_3CHOH^{\bullet+}CH_3)$ of 4 kJ mol^{-1} (Table 1). The critical energies derived by theory are again higher than ones obtained by PI, also attributable to a very long CC bond at the B3LYP/6-311G(d,p) optimum geometry (Table 4). This configuration is 40 kJ mol^{-1} more stable than $CH_3CH(OH^{\bullet+})CH_3$ is at the optimum geometry of the neutral. Although not as nicely as for $CH_3CH_2OH^{\bullet+}$, correcting the PI dissociation energies for this Franck–Condon energy reduced somewhat the discrepancy between experiment and DFT results.

Five of the ground state vibrational frequencies were markedly lowered in the DFT transition state for the loss of $CH_3^\bullet$ from $CH_3CH(OH^{\bullet+})CH_3$. These modes correspond to rotations of partners in the intermediate complex and become translations and rotations of the partners upon complete separation. Similarly to the loss of $H^\bullet$ from $CH_3CH_2OH^{\bullet+}$, the DFT values of the vibrational frequencies for the transition state for $H^\bullet$ loss from $CH_3CH(OH^{\bullet+})CH_3$ changed little from those for the ground state ion (Table 6). Thus, as in the corresponding dissociation of CH_3 $CH_2OH^{\bullet+}$, this transition state is much tighter than that for $CH_3^\bullet$ loss.

3.3. $CH_3CH(OH^{\bullet+})CH_2CH_3$

A transition state for $H^\bullet$ loss from $CH_3CH(OH^{\bullet+})$ CH_2CH_3 was located by DFT 5 kJ mol^{-1} below the energy of the products, and one for $C_2H_5^\bullet$ loss was found 21–23 kJ mol^{-1} below the corresponding products. A transition state for the loss of $CH_3^\bullet$ was not located by either B3LYP/6-31G(d) or B3LYP/6-311g(d,p) theory, despite substantial effort. As in other systems examined, there were only modest changes in DFT vibrational frequencies between the ground state and the transition state for $H^\bullet$ loss, whereas six of the frequencies in the transition state found for loss of $C_2H_5^\bullet$ were markedly lowered from their values in the ground state (Table 6). $CH_3CH(OH^{\bullet+})C_2H_5$ is 70 kJ mol^{-1} more stable at its optimum DFT geometry than it is at the DFT geometry of the neutral

molecule. Correcting for this gives values that overestimate the difference between experiment and theory by an amount equal and opposite to the difference without correction. This suggests that the calculated Franck–Condon corrections are excessive in this case.

3.4. $CH_3C(=O^{\bullet+})C_2H_5$

DFT placed the transition state for $CH_3^\bullet$ loss 0.4–2 kJ mol^{-1} below the energy of the corresponding products, and the transition state for $C_2H_5^\bullet$ loss 5–8 kJ mol^{-1} below its products. The DFT onsets for $CH_3^\bullet$ and $C_2H_5^\bullet$ losses are at essentially the same energy, whereas AE(–$CH_3^\bullet$) is 20 kJ mol^{-1} below AE(–$C_2H_5^\bullet$) (Table 1). The breaking CC bonds in the DFT transition states for both alkyl losses from the 2-butanone ion were very long (Table 4). As in the systems characterized above, correcting the PI critical energy for the stabilization arising from post ionization C–CH_2CH_3 bond lengthening (14 kJ mol^{-1}) brought the PI and DFT dissociation energies much closer together. Thus, post-ionization bond lengthening again appears to be the largest source of the discrepancies between the DFT and PI dissociation energies. Eight B3LYP/6-31G(d) frequencies of the 2-butanone ion were lowered markedly in both transition states (Table 6).

4. RRKM calculations

RRKM calculations were performed using assorted models to determine the features required in the transition states to reproduce the higher energy experimental results. Because DFT transition states were not found for all reactions, we employed transition state energies based on PIAE data in RRKM calculations throughout this work. Critical energies were corrected for the effect of long bond formation observed by DFT theory in ground state reactant ions in some calculations on every dissociation. Although other models were evaluated, correcting activation energies for subthreshold bond-breaking and Franck–Condon effects seems most reasonable based on the foregoing. B3LYP/6-31G(d) frequencies were used in all RRKM calculations, except five or more DFT transition state frequencies (usually ones that became rotations and translations upon alkyl loss) were tightened or treated as free rotors in alkyl losses in some models because of an inability to locate transition states for some of the dissociations by DFT and doubts about whether the transition states that were located by DFT are actually rate determining. Thus, for RRKM calculations, we used the frequencies of the dissociated partners and typically represented the transitional modes by five additional frequencies adjusted to reproduce the behavior of the FDPI curves. These frequencies are the only parameters arbitrarily adjusted in these studies. The estimated frequencies were always higher than the lowest frequencies in the DFT transition states (Table 6), so the adjusted frequencies gave tighter transition states.

4.1. $CH_3CH_2OH^{\bullet+}$

RRKM theory was used to calculate the rates of $H^\bullet$ and $CH_3^\bullet$ loss from $CH_3CH_2OH^{\bullet+}$ as a function of ion internal energy. In one set of calculations for methyl loss, the transition state energy was taken as AE(products) minus the ionization energy (IE) of ethanol, and the transition state frequencies were taken to be those obtained by DFT for the separated partners. The remaining five frequencies in this transition state were treated as free rotors. This gave a rate of $CH_3^\bullet$ loss about five orders of magnitude faster at its threshold than $H^\bullet$ loss at the same energy and an even greater discrepancy at higher energies, poorly reproducing the similar rates of the two reactions. A second calculation was carried out in which the transition state energies used in the first calculation were raised by the stabilization energy for long bond formation, and the transition state energy for loss of $CH_3^\bullet$ was lowered by the 12 kJ mol^{-1} difference between the appearance energies for losses of $CH_3^\bullet$ and CH_4 from $CH_3CH(OH^{\bullet+})CH_3$. Five free rotors were used in this transition state for $CH_3^\bullet$ loss. In this calculation, the rate of $CH_3^\bullet$ loss rose to several orders of magnitude faster than that of $H^\bullet$ loss at higher

energies, i.e., above threshold the rate of the former rose more rapidly than that of the latter. Furthermore, k for $CH_3^\bullet$ loss rose above $1 \times 10^{14}\,s^{-1}$, impossibly fast.

Tightening the methyl loss transition state by making the five lowest energy frequencies all $125\,cm^{-1}$ in addition to subtracting $12\,kJ\,mol^{-1}$ energy to correct for bond cleavage below the dissociation threshold and adding $34\,kJ\,mol^{-1}$ for the lowered ground state energy due to long bond formation caused $CH_3^\bullet$ loss to surpass the loss of $H^\bullet$ at about $70\,kJ\,mol^{-1}$ above the onset of the latter with the two rates staying within an order of magnitude at higher energies (Fig. 6). (See the discussion for $CH_3CH(OH^{\bullet+})CH_3$ that follows for justification of this estimation of the transition state energy.) This calculation reasonably reproduced the relative abundances of the FDPI curves (Fig. 1). Throughout this work, RRKM calculations assuming transition states below the dissociation thresholds generally gave better agreement with the FDPI curves than did omitting that correction. Markedly improved agreement between RRKM results and experiment was also obtained previously when ab initio energies for a long-bonded *n*-propanol ion rather than experimental dissociation energies were used in RRKM calculations [55].

The tightening of the transition state frequencies needed to obtain reasonable absolute and relative rates for the two dissociations of $CH_3CH_2OH^{\bullet+}$ indicates that the rate-controlling transition state for the loss of $CH_3^\bullet$ is significantly earlier (perhaps coinciding with one close to that for ion–neutral complex formation) than the DFT transition state. Rate constants considering the combined effects of the two transition states were calculated using the following formula [56].

$$k = \frac{N_{ti}}{h\rho}\left(\frac{N^{\#}_{dis}}{N^{\#}_{ti} + N^{\#}_{dis}}\right)$$

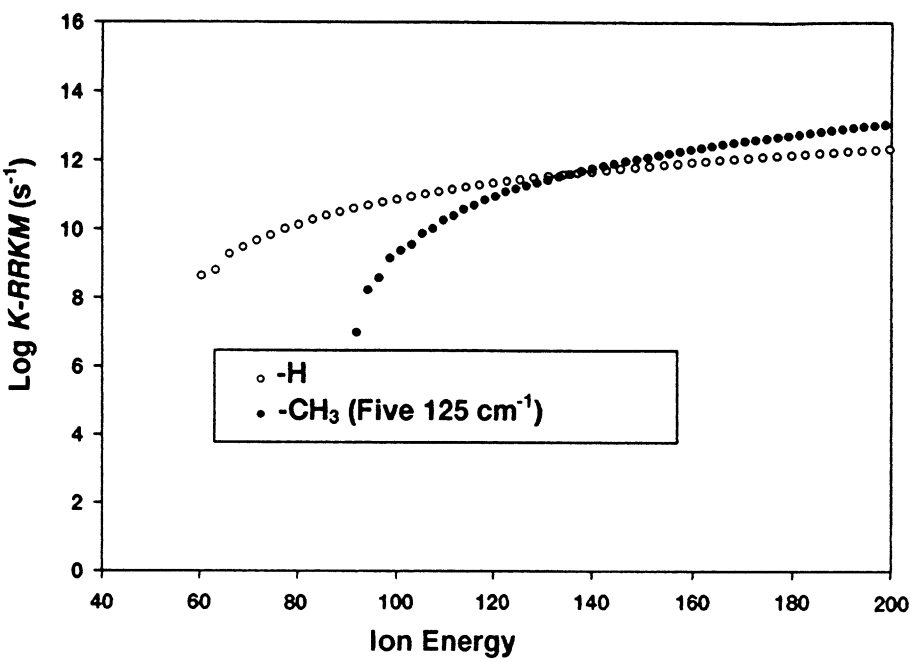

Fig. 6. RRKM plots of log rate constant (k) vs. ion internal energy for dissociations of $CH_3CH_2OH^{\bullet+}$. The curves were obtained using PI energies corrected for post-ionization stabilization of the ground state ion based on results of DFT theory and subthreshold cleavage of the CC bond (see text). $H^\bullet$ loss transition state frequencies were those for the by DFT transition state. Transition state frequencies for methyl loss were taken to be those of the separated products with the five additional frequencies for $CH_3^\bullet$ loss (Table 4) made $125\,cm^{-1}$ to obtain reasonable agreement between the rates of the two reactions.

where N_{ti} is the sum of states for the tight transition state and N_{dis} is the sum of states for the loose transition state. The early transition state very quickly becomes rate determining for this dissociation because calculating the rate of dissociation at 1 kJ mol^{-1} above the dissociation threshold and considering the combined effects of the two transition states (taken to be the tight and DFT transition states) gave a dissociation rate that is 100% of the rate obtained by considering only the tight transition state. The range of the corresponding percentages at $\leq$1 kJ mol^{-1} above threshold was 96–99% for the other alkyl losses studied. All of these percentages increased with increasing energy. Therefore, RRKM rate curves given considered only the tight TSs.

The more rapid rise in the rate of $CH_3^\bullet$ loss than of $H^\bullet$ loss with increasing energy can be attributed to marked decreases in frequencies of the five modes that are becoming rotations and translations during the loss of $CH_3^\bullet$, in conjunction with the small changes in the frequencies in the transition state for the loss of $H^\bullet$ from the corresponding ground state frequencies (Table 6). The DFT transition state energies, frequencies and lengths of breaking bonds suggest that the CH bond is broken earlier and more abruptly than is the CC bond. This probably reflects the weaker ion-induced dipole attractions between the separating fragments in the former than in the latter dissociation.

4.2. $CH_3CH(OH^{\bullet+})CH_3$

Our first RRKM calculations of the rates of dissociation of $CH_3CH(OH^{\bullet+})CH_3$ as a function of ion internal energy employed the PI thresholds for dissociation energies and the vibrational frequencies of the separated products. In that model, the frequencies other than the reaction coordinate that become rotations or translations upon dissociation were treated as free rotors in the transition states. In the second model, the difference between the energies of the molecular ion in its DFT optimum geometry and in the geometry of the neutral was added to the dissociation energy for methane elimination. In a final calculation, the critical energy was corrected assuming the long-bonded DFT ground state and the transition state taken to be at the threshold for methane elimination, and the five lowest transition state frequencies for $CH_3^\bullet$ loss were assigned values of 150 cm^{-1} rather than the DFT frequencies or being treated as free rotors (other frequencies were those of the dissociated partners).

All of the RRKM models produced a more rapid increase in $CH_3^\bullet$ than $H^\bullet$ loss from $CH_3CH(OH^{\bullet+})CH_3$ with increasing energy. This was again due to the low transition state frequencies or internal rotations used in the methyl loss transition state in these models vs. the high DFT frequencies in the transition state for $H^\bullet$ loss. In the first two models, $CH_3^\bullet$ loss quickly became 2–3 orders of magnitude faster than $H^\bullet$ loss (Fig. 7), markedly exceeding the difference between the FDPI curves. The rate for $CH_3^\bullet$ loss in the second model reached 10^{17} s^{-1}, a physically unrealistic rate. This, together with the excessively high rates of $CH_3^\bullet$ loss relative to those for $H^\bullet$ loss, suggests that this DFT transition state for $CH_3^\bullet$ loss is "looser" than the actual transition state. Arbitrarily making the lowest DFT frequencies in the RRKM calculations for the rate of $CH_3^\bullet$ loss 150 cm^{-1} gave reasonable absolute and relative rates for this reaction (Fig. 7). The need to substantially tighten the transition state for $CH_3^\bullet$ loss relative to the B3LYP/6-31G(d) transition state is evidence that the rate-limiting transition state occurs before the partners begin to rotate relative to one another.

It is well established that alkane eliminations occur in two steps: (1) CC bond cleavage to form a complex followed by (2) $H^\bullet$ transfer between the partners to complete the reaction [6,39]. Furthermore, once a CC bond cleaves to form a complex, alkane elimination appears to be much faster than reformation of the CC bond [32,57], making alkane elimination a measure of the rate of CC bond cleavage below the threshold for simple alkyl loss. The greater PI loss of CH_4 than $H^\bullet$ at low energy supports the reality of the faster RRKM rate of CC than of CH cleavage even below the threshold for complete dissociation to $CH_3^\bullet + CH_3CH{=}OH^+$ when the lowered transition state energy for that process was used, consistent

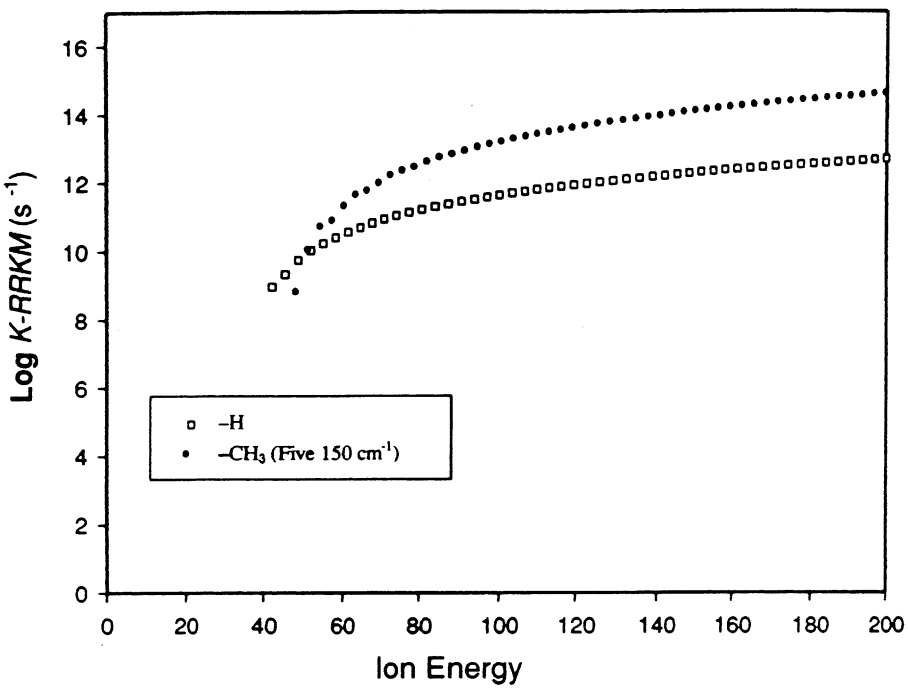

Fig. 7. RRKM plots of log(*k*) vs. ion internal energy for dissociations of $CH_3CH(OH^{\bullet+})CH_3$. The curves were obtained using PI energies corrected for post-ionization stabilization of the ground state ion and subthreshold cleavage of the CC bond. Frequencies were obtained as for $CH_3CH_2OH^{\bullet+}$ (legend for Fig. 6).

with the validity of this model. This implies more frequent CC than CH bond cleavage at all energies above the threshold for forming the $[CH_3CH{=}OH^+\ CH_3^{\bullet}]$ complex (Fig. 2), even those below the threshold for complete dissociation of the fragments.

4.3. $CH_3CH(OH^{\bullet+})C_2H_5$

As in the preceding systems, using transition states containing free rotors and lack of correction of the transition state energies for long-bond formation gave rates of alkyl losses much faster than did using the corrected FDPI energies. Correcting critical energies for stabilization of the DFT ground state and placing transition state energies for alkyl losses at the thresholds for alkane eliminations gave rate curves in good agreement with FDPI curves, and utilizing B3LYP frequencies for the separated partners except making the six lowest frequencies in the transition state for $CH_3^{\bullet}$ loss 125 cm^{-1} gave a curve for $CH_3^{\bullet}$ loss that crossed over that for $H^{\bullet}$ loss, becoming about one order of magnitude faster when the internal energy reached 200 kJ mol^{-1} (Fig. 8). Using five 100 cm^{-1} frequencies in the transition state for the $CH_3CH_2^{\bullet}$ loss to represent those being transformed to vibrations and rotations gave approximate agreement between theory and experiment among the three FDPI curves. At higher energies the curve for $C_2H_5^{\bullet}$ loss obtained with 100 cm^{-1} frequencies crossed over that obtained for $CH_3^{\bullet}$ loss using 125 cm^{-1} frequencies (Fig. 8), in agreement with observations (Fig. 3). As for the preceding ions, it is likely that entropic bottlenecks rather than saddle points such as those found by the DFT calculations are rate determining. Since tightening the low energy frequencies more for the losses of smaller alkyl groups was the only plausible way to obtain similar results between experiment and RRKM theory, the results imply that larger alkyl groups are lost

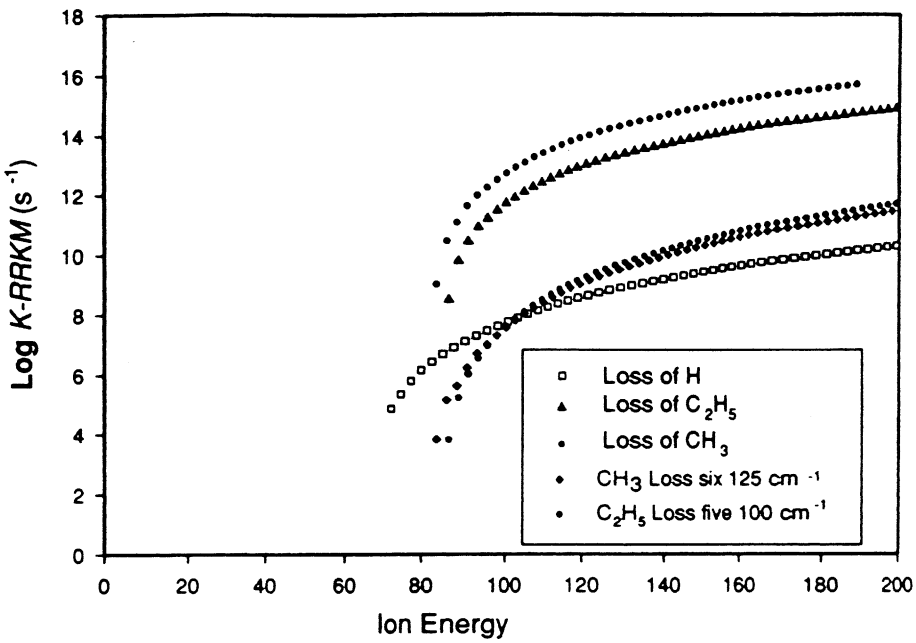

Fig. 8. RRKM plots of log(k) vs. ion internal energy for dissociations of $CH_3CH(OH^{\bullet+})CH_2CH_3$. The critical energies were obtained using PI energies corrected for post-ionization stabilization of the ground state ion and subthreshold cleavage of the CC bond. The upper curves for $CH_3^{\bullet}$ and $CH_3^{\bullet}$ losses were obtained assuming five free rotors in the transition states. The lower curves were obtained by making the six lowest frequencies in the transition state for $CH_3^{\bullet}$ loss 125 cm^{-1} and the five lowest frequencies in the transition state for $CH_3CH_2^{\bullet}$ 100 cm^{-1}. Other frequencies were obtained as described in the text.

preferentially at higher energies because their transition states are looser.

4.4. $CH_3C(=O^{\bullet+})CH_2CH_3$

RRKM calculations that gave results for the dissociations of the 2-butanone ion most like the FDPI curves employed frequencies for the B3LYP/6-31G(d) transition state with transition state energies that were lowered from the experimental ones by the same amounts as were those for the corresponding reactions of the 2-butanol ion and raised by the addition of 14 kJ mol^{-1}, the DFT difference between the stability of the long-bonded ion and that of the ion in the geometry of the neutral. Differences between thresholds for alkyl losses and alkane eliminations from the 2-butanol ion were used to estimate corrections for locating the transition states for the corresponding alkyl losses because alkane eliminations from the 2-butanone ion are insignificant [58]. The RRKM log rate constant vs. energy curves were close to each other in this model. However, the rates at higher energies were unrealistically fast.

RRKM calculations utilizing five 175 cm^{-1} frequencies as the lowest ones for the $CH_3^{\bullet}$ loss and five 100 cm^{-1} frequencies for the $CH_3CH_2^{\bullet}$ loss gave a rate of $CH_3CH_2^{\bullet}$ loss that reached and surpassed that of $CH_3^{\bullet}$ loss at high energies (Fig. 9). This reproduced the more rapid FDPI rise of the rate of $C_2H_5^{\bullet}$ loss relative to that for $CH_3^{\bullet}$ loss with increasing energy (Fig. 8) and the favored loss of $C_2H_5^{\bullet}$ upon 70 eV electron impact. The RRKM results suggest that, as in the alcohol ions, the rate determining transition states for alkyl losses are earlier and tighter than those obtained by DFT. Also as with $CH_3CH(OH^{\bullet+})CH_2CH_3$, the requirement for a looser transition state for loss of $CH_3CH_2^{\bullet}$ to reproduce dominance of that fragmentation at higher energies is evidence that looser

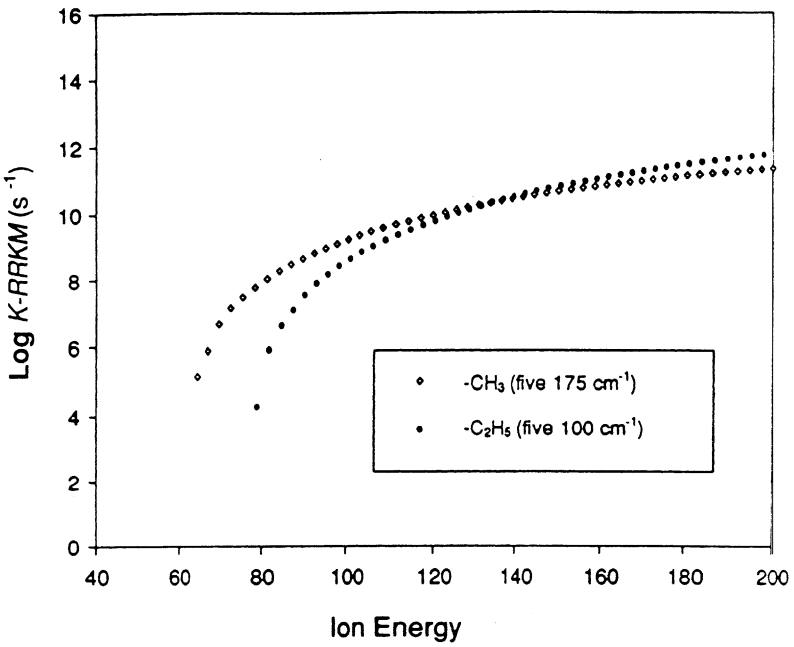

Fig. 9. RRKM rates for the losses of $CH_3^\bullet$ (*m*/*z* 57) and $C_2H_5^\bullet$ (*m*/*z* 43) from the 2-butanone ion as a function of energy. The curves were obtained using PI energies corrected for post-ionization stabilization of the ground state ion and subthreshold cleavage of the CC bond (see text). The five lowest frequencies were made 175 cm^{-1} for $CH_3^\bullet$ for $CH_3^\bullet$ loss and 100 cm^{-1} for $CH_3CH_2^\bullet$ loss. Note that methyl loss dominates near threshold, but that the $C_2H_5^\bullet$ loss becomes more important at higher energies.

transition states cause loss of larger alkyl groups to be preferred at higher energies. Thus, looser transition states for losses of larger alkyl groups appear to be the general explanation for the more abundant losses of larger alkyl groups at higher energies, despite the higher onsets for those dissociations.

Our experiments do not directly address the effect of angular momentum. However, angular momentum is likely to have significant effects only when the transition states are for the full dissociation of the partners [25], which is not the case for the reactions compared here. Except perhaps very close to threshold, our RRKM model adequately accounts for the experimental branching ratios.

5. Summary

Present results display good agreement between energies obtained by experimental measurements and DFT theory when CC bond lengthening is taken into account, supporting the accuracy of both. The only arbitrary adjustments used in the RRKM calculations were the lowest frequencies in the transition states for alkyl losses. Experimental breakdown diagrams were much better reproduced by RRKM theory when the rate-determining transition states for alkyl losses were placed below the actual dissociation thresholds. Thus, it is likely that this is a feature of an accurate and realistic model. Improving the results would require an accuracy for both experiment and theory of the order of 1 kJ mol^{-1}, an accuracy that is difficult to achieve in either the experimental or theoretical approaches currently available.

Present results establish the generalization that $H^\bullet$ losses from radical cations in the gas phase are slow and increase very slowly with increasing internal energy. This is attributed to their vibrational frequencies changing little between the ground and transition states, causing the sum of states/density of states ratio

in RRKM theory to increase slowly with increasing *E*. In contrast, the vibrational frequencies in transition states for alkyl losses that become rotations and translations of fragments are substantially lowered in those transition states. The contrast between transition state frequencies for H and alkyl losses is attributable to (1) the creation of three additional rotational degrees of freedom in the latter but not the former type of reaction, and (2) the greater long range attractions between alkyl fragments and ions. Therefore, alkyl losses increase more rapidly in rate with increasing energy than do those for $H^{\bullet}$ loss from ions in the gas phase. It is predicted from this that tighter transition states cause all losses of atoms in the gas phase to be slow relative to losses of larger fragments by simple cleavages. However, establishing the validity of this generalization requires measurements on losses of atoms other than $H^{\bullet}$ and on dissociations of neutral molecules.

Near threshold, losses of smaller alkyls are favored relative to losses of larger ones because the former are energetically favored. However, the losses of the larger alkyls increase more rapidly and become dominant with increasing energy because they have looser transition states. This is supported by the formation of long CC bonds to alkyl groups even in the ground state; the bond is lengthened to the larger alkyl group when there are differing alkyl substituents on the alpha carbon. Present work suggests that long bonds in the ground states, transition states for CC bond breaking to the larger alkyl group being further below the threshold for dissociation and preferred loss of larger alkanes are related phenomena. Locating transition states using ab initio theory to obtain energies, geometries and frequencies together with variational RRKM theory demonstrated a longer CC bond, a higher energy and lower vibrational frequencies in the minimum entropy transition states for loss of ethyl vs. propyl from the 3-hexylamine radical cation [27], as inferred in present work. Although it may seem paradoxical that the reactions with the looser, lower energy transition states have higher thresholds for dissociation, the latter can be attributed to stronger ion-induced dipole attractions and weaker covalent forces in those breaking bonds.

6. Methods

Photoionization efficiency curves, first differential curves derived from them and PI appearance energies were obtained as described previously [33,59] on a mass spectrometer fitted with a photoionization source [60]. Photoionization experiments were carried out at room temperature. The PI signals were corrected for variation in photon flux as a function of energy by multiplying by: (ion count rate − background ion count rate)/(photon count rate – background photon count rate). First differential curves provided ion abundances as a function of molecular ion internal energy [31,32]. RRKM rates were calculated using the program of Zhu and Hase [61]. The GAUSSIAN 94 package [62] was used for B3LYP/6-31G(d), B3LYP/6-311G(d,p) and QCISD levels of theory. Ground state geometries were identified in all cases by having only real vibrational frequencies. All DFT transition states described had only one imaginary frequency, and all DFT vibrational frequencies were multiplied by 0.9614 for use in RRKM calculations, and by 0.9806 when used for zero point vibrational energy corrections [63].

Acknowledgements

The financial assistance of the Australian Research Council and the technical assistance of Xia (Thomas) Chen are gratefully acknowledged.

References

[1] P. Longevialle, R. Botter, J. Chem. Soc. Chem. Commun. (1980) 823.
[2] P. Longevialle, R. Botter, Int. J. Mass Spectrom. Ion Phys. 47 (1983) 179.
[3] P. Longevialle, O. Lefevre, Org. Mass Spectrom. 28 (1993) 1083.
[4] P. Longevialle, Rapid Comm. Mass Spectrom. 9 (1995) 1189.
[5] T.H. Morton, Tetrahedron 38 (1982) 3195.
[6] D.J. McAdoo, Mass Spectrom. Rev. 7 (1988) 363.
[7] R.D. Bowen, Accts. Chem. Res. 24 (1991) 364.
[8] P. Longevialle, Mass Spectrom. Rev. 11 (1992) 157.
[9] D.J. McAdoo, T.H. Morton, Accts. Chem. Res. 26 (1993) 295.
[10] J.T.B. Marshall, D.H. Williams, Tetrahedron 23 (1967) 321.

[11] W. Carpenter, A.M. Duffield, C. Djerassi, J. Am. Chem. Soc. 89 (1967) 6167.
[12] R.G. Cooks, A.N.H. Yeo, D.H. Williams, Org. Mass Spectrom. 2 (1969) 985.
[13] R.D. Bowen, P. Clifford, J.T. Francis, J.K. Terlouw, Int. J. Mass Spectrom. Ion Processes 156/166 (1997) 155.
[14] A. Maccoll, Org. Mass Spectrom. 16 (1981) 297.
[15] A.B. King, J. Chem. Phys. 42 (1965) 3526.
[16] C. Lifshitz, J. Phys. Chem. 87 (1983) 2304.
[17] W. Carpenter, A.M. Duffield, C. Djerassi, J. Am. Chem. Soc. 90 (1968) 160.
[18] C.E. Hudson, D.J. McAdoo, Org. Mass Spectrom. 14 (1979) 109.
[19] G. Bouchoux, R. Flammang, Y. Hoppilliard, P. Jaudon, A. Maquestiau, P. Meyrant, Spectrosc. Int. J. 3 (1984) 1.
[20] D.J. McAdoo, C.E. Hudson, F.W. McLafferty, T.E. Parks, Org. Mass Spectrom. 19 (1984) 353.
[21] R.D. Bowen, J. Chem. Soc. Perkin Trans. II (1990) 147.
[22] D.J. McAdoo, S. Olivella, A. Sole, J. Phys. Chem. A 52 (1998) 10798.
[23] G.G. Meisels, G.M.L. Verboom, M.J. Weiss, T.C. Hsieh, J. Am. Chem. Soc. 101 (1979) 7189.
[24] W.J. Chesnavich, L. Bass, T. Su, M.T. Bowers, J. Chem. Phys. 74 (1981) 2228.
[25] M.T. Bowers, M.F.J. Jarrold, W. Wagner-Redeker, P.R. Kemper, L.M. Bass, Faraday Disc. Chem. Soc. 75 (1983) 57.
[26] J.A. Booze, M. Schweinsberg, T. Baer, J. Chem. Phys. 99 (1993) 4441.
[27] S. Hammerum, T.L. Sølling, T. Vulpius, in: Proceedings of the 15th International Mass Spectrometry Conference, 2000.
[28] W.L. Hase, Acc. Chem. Res. 16 (1983) 258.
[29] A.D. Becke, J. Chem. Phys. 98 (1993) 5648.
[30] B.J. Smith, L. Radom, Chem. Phys. Lett. 231 (1994) 345.
[31] H. Hurzeler, M.G. Inghram, J.D. Morrison, J. Chem. Phys. 28 (1958) 76.
[32] J.C. Traeger, C.E. Hudson, D.J. McAdoo, J. Am. Soc. Mass Spectrom. 7 (1995) 73.
[33] J.C. Traeger, R.G. McLoughlin, J. Am. Chem. Soc. 103 (1981) 3647.
[34] C.E. Hudson, L. DeLeon, D. Van Alstyne, D.J. McAdoo, J. Am. Soc. Mass Spectrom. 5 (1994) 1102.
[35] E. Uggerud, T. Helgaker, J. Am. Chem. Soc. 114 (1992) 4265.
[36] J.L. Holmes, P.C. Burgers, Y.A. Mollah, Org. Mass Spectrom. 17 (1982) 127.
[37] S. Hammerum, K.F. Donchi, P.J. Derrick, Int. J. Mass Spectrom. Ion Phys. 47 (1983) 347.
[38] A.J. Chalk, L. Radom, J. Am. Chem. Soc. 120 (1998) 8430.
[39] D.J. McAdoo, R.D. Bowen, Eur. Mass Spectrom. 5 (1999) 389.
[40] J.D. Shao, T. Baer, D.L. Lewis, J. Phys. Chem. 92 (1988) 5123.
[41] J.C. Traeger, C.E. Hudson, D.J. McAdoo, J. Phys. Chem. 92 (1988) 1519.
[42] D.J. McAdoo, C.E. Hudson, J.C. Traeger, A. Grose, L.L. Griffin, J. Am. Soc. Mass Spectrom. 2 (1991) 261.
[43] P.T. Mead, K.F. Donchi, J.C. Traeger, J.R. Christie, P.J. Derrick, J. Am. Chem. Soc. 102 (1980) 3364.
[44] K.M. Weitzel, J.A. Booze, T. Baer, Chem. Phys. 150 (1991) 263.
[45] S. Olivella, A. Sole, D.J. McAdoo, L.L. Griffin, J. Am. Chem. Soc. 11 (1994) 11078.
[46] E. Stenhagen, S. Abrahamsson, F.W. McLafferty, Atlas of Mass Spectral Data, Interscience Publishers, New York, 1969.
[47] D.P. Stevenson, Disc. Faraday Soc. 10 (1951) 35.
[48] H.E. Audier, Org. Mass Spectrom. 2 (1969) 283.
[49] D.J. McAdoo, Mass Spectrom. Rev. 19 (2000) 38.
[50] C. Lifshitz, F. Louage, V. Aviyente, K. Song, J. Phys. Chem. 95 (1991) 9298.
[51] T.H. Morton, Org. Mass Spectrom. 27 (1992) 353.
[52] J.W. Gauld, L. Radom, Chem. Phys. Lett. 275 (1997) 28.
[53] W.J. Bouma, D. Poppinger, L. Radom, Isr. J. Chem. 23 (1983) 21.
[54] J.A. Booze, T. Baer, J. Phys. Chem. 96 (1992) 5710.
[55] J.A. Booze, T. Baer, J. Phys. Chem. 96 (1992) 5715.
[56] T. Baer, W.L. Hase, Unimolecular Reaction Dynamics: Theory and Experiments, Oxford University Press, New York, 1996, p. 276.
[57] M.S. Ahmed, C.S. Giam, D.J. McAdoo, Int. J. Mass Spectrom. Ion Processes 130 (1994) 1.
[58] C.E. Hudson, M.S. Ahmed, S. Olivella, C.S. Giam, D.J. McAdoo, Org. Mass Spectrom. 27 (1992) 435.
[59] J.C. Traeger, T.H. Morton, J. Am. Chem. Soc. 118 (1996) 9661.
[60] J.C. Traeger, Int. J. Mass Spectrom. Ion Processes 58 (1984) 259.
[61] T.L. Zhu, W.L. Hase, A general RRKM program, Quantum Chemistry Program Exchange, Chemistry Department, University of Indiana, Bloomington, IN QCPE 644, 1993.
[62] M.J. Frisch, G.W. Trucks, H.B. Schlegel, P.M.W. Gill, B.G. Johnson, M.A. Robb, J.R. Cheeseman, T. Keith, G.A. Petersson, J.A. Montgomery, K. Raghavachari, M.A. Al-Laham, V.G. Zakrzewski, J.V. Ortiz, J.B. Foresman, J. Cioslowski, B.B. Stefanov, A. Nanayakkara, M. Challacombe, C.Y. Peng, P.Y. Ayala, W. Chen, M.W. Wong, J.L. Andres, E.S. Replogle, R. Gomperts, R.L. Martin, D.J. Fox, J.S. Binkley, D.J. Defrees, J. Baker, J.P. Stewart, M. Head-Gordon, C. Gonzalez, J.A. Pople, GAUSSIAN 94 Revision E.2, Gaussian, Inc., Pittsburgh, PA, 1995.
[63] A.P. Scott, L. Radom, J. Phys. Chem. 100 (1996) 16502.
[64] C. Traeger, B.M. Kompe, in: J.A.M. Simoes, A. Greenburg, J.F. Liebman (Eds.), Energetics of Organic Radicals, Chapman and Hall, London, 1996, pp. 59–109.
[65] E.P.L. Hunter, S.G. Lias, J. Phys. Chem. Ref. Data 27 (1998) 413–656.
[66] J.C. Traeger, M. Djordjevic, Eur. J. Mass Spectrom. 5 (1999) 319–324.
[67] S.G. Lias, J.E. Bartmess, J.F. Liebman, J.L. Holmes, R.D. Levin, W.G. Mallard, Gas Phase Neutral Thermochem. 17 (1988) 1–169.
[68] J.C. Traeger, in: Proceedings of the 48th ASMS Conference on Mass Spectrometry and Allied Topics, Long Beach, CA, 11–15 June 2000, ThPH 284.
[69] M.T. Nguyen, H.M.T. Nguyen, Chem. Phys. Lett. 300 (1999) 346–350.